

Hard X-rays and Fluorescent Iron Emission from the Embedded Infrared Cluster in NGC 2071

Stephen L. Skinner, Audrey E. Simmons

CASA, Univ. of Colorado, Boulder, CO, USA 80309-0389

Marc Audard

Integral Science Data Centre, Ch. d'Ecogia 16, CH-1290 Versoix, Switzerland

Geneva Observatory, University of Geneva, Ch. des Maillettes 51, 1290 Sauverny, Switzerland

Manuel Güdel

Paul Scherrer Institute, Würenlingen and Villigen, CH-5232 Switzerland

ABSTRACT

We present first results of *XMM-Newton* X-ray observations of the infrared cluster lying near the NGC 2071 reflection nebula in the Orion B region. This cluster is of interest because it is one of the closest regions known to harbor embedded high-mass stars. We report the discovery of hard X-ray emission from the dense central NGC 2071-IR subgroup which contains at least three high-mass young stellar objects (NGC 2071 IRS-1, IRS-2, and IRS-3). A prominent X-ray source is detected within $1''$ of the infrared source IRS-1, which is thought to drive a powerful bipolar molecular outflow. The X-ray spectrum of this source is quite unusual compared to the optically thin plasma spectra normally observed in young stellar objects (YSOs). The spectrum is characterized by a hard broadband continuum plus an exceptionally broad emission line at ≈ 6.4 keV from neutral or near-neutral iron. The fluorescent Fe line likely originates in cold material near the embedded star (i.e. a disk or envelope) that is irradiated by the hard heavily-absorbed X-ray source.

Subject headings: open clusters and associations: individual (NGC 2071) — stars: formation — X-rays: stars

1. Introduction

A high-mass star can arrive on the main-sequence completely enshrouded in dust and inaccessible to optical studies. Thus, the ability to penetrate high extinction is crucial to exploring the earliest stages of high-mass star formation. Infrared, radio, and millimeter observations have traditionally been used and provide important information on physical conditions in circumstellar disks and envelopes or in ionized winds or HII regions around the massive young star. X-ray observations can also penetrate high extinction and provide a different perspective that probes high-energy processes including magnetic activity originating close to the stellar surface, mass-loss as traced by shocked winds, jets, or outflows, and hot diffuse gas that pervades some young clusters containing massive young OB stars with powerful winds.

One of the closest regions known to contain young high-mass stars is the infrared cluster near the optical reflection nebula NGC 2071 in the Orion B region (Lynds 1630 dark cloud) at a distance of ~ 400 pc (Anthony-Twarog 1982; Brown et al. 1994). Near-infrared observations by Lada et al. (1991) revealed more than 100 K-band sources in a 100 arc-min^2 region down to $K \approx 14$ mag. This extended cluster surrounds a dense central subgroup known as NGC 2071-IR which contains at least 10 near-IR sources in a $\approx 1' \times 1'$ region (Walther et al. 1993 = Wa93). Of particular interest in the NGC 2071-IR subgroup are IRS-1, IRS-2, and IRS-3. These sources are surrounded by compact HII regions (Snell & Bally 1986) and H_2O and OH masers lie in proximity. More detailed information on NGC 2071-IR and properties of the infrared sources can be found in Aspin, Sandell, & Walther (1992) and Wa93, and references therein. The presence of strong ionizing UV radiation and maser emission strongly suggests that these objects are young embedded early-type stars. Such objects are exceedingly rare at distances less than 500 pc and the NGC 2071 cluster thus plays a key role in observational studies of high-mass star formation.

We report here on first results of a pointed X-ray observation of NGC 2071 obtained with *XMM-Newton*. This observation is centered on the NGC 2071-IR subgroup and provides broader energy coverage and improved spectral information compared to two previous ROSAT HRI exposures (rh202521/22) which captured the IR subgroup $\approx 8' - 10'$ off-axis. Our objectives were to (i) obtain an X-ray census of the NGC 2071 cluster and (ii) search for X-ray emission from the massive embedded stars, whose X-ray properties are largely unknown. We report the detection of hard emission lying within $1''$ of NGC 2071-IRS1 and discuss its very unusual X-ray spectrum which is dominated by strong fluorescent Fe line emission.

2. XMM-Newton Observations

The *XMM-Newton* observation began on 2005 March 30 at 15:20 UT and ended on March 31 at 03:53 UT. Pointing was centered on NGC 2071-IRS 1 (Wa93). The European Photon Imaging Camera (EPIC) provided CCD imaging spectroscopy from the pn camera (Strüder et al. 2001) and two nearly identical MOS cameras (MOS1 and MOS2; Turner et al. 2001). The medium optical blocking filter was used. The EPIC cameras provide energy coverage over $E \approx 0.2 - 15$ keV with energy resolution $E/\Delta E \approx 20 - 50$. The MOS cameras provide the best on-axis angular resolution with FWHM $\approx 4.3''$ at 1.5 keV.

Data were reduced using the *XMM-Newton* Science Analysis System (SAS vers. 6.1). Event files generated by *XMM-Newton* standard processing were time-filtered to remove the first ≈ 15 ksec of data, which were affected by high background radiation. This yielded 29.9 ksec of usable pn exposure and 30.1 ksec of usable exposure per MOS. Source detection was accomplished with the SAS task *edetect_chain* on images filtered in different bands. These results were compared with the source list provided from the *XMM-Newton* pipeline processing and images were visually checked for missed or spurious detections. The properties of sources detected in the central cluster region (Table 1) are based on events in the 0.5 - 7.5 keV range.

Spectra and light curves were extracted from circular regions of radius $R_e = 15''$ centered on individual sources, corresponding to $\approx 68\%$ encircled energy at 1.5 keV. Smaller regions were used for a few closely spaced sources to avoid region overlap. Background files were extracted from circular source-free regions near the source. The SAS tasks *rmfgen* and *arfgen* were used to generate source-specific response matrix files (RMFs) and auxiliary response files (ARFs) for spectral analysis. The data were analyzed using the *XANADU* software package ¹, including *XSPEC* vers. 12.3.0.

3. X-ray Overview of NGC 2071

Figure 1 shows a broad-band 0.5 - 7 keV EPIC pn image of the central $\approx 10' \times 10'$ cluster region surrounding the NGC 2071-IR subgroup. Analysis of both the pn and MOS images resulted in 33 X-ray detections in this central region, as summarized in Table 1. Possible counterparts were found for 23 of these 33 sources (70%) within a search radius of $2''$ using

¹The *XANADU* X-ray analysis software package is developed and maintained by NASA's High Energy Astrophysics Science Archive Research Center (HEASARC). See <http://heasarc.gsfc.nasa.gov/docs/xanadu/xanadu.html> for further information.

the 2MASS, HST GSC v2.2, and USNO B1 electronic data bases. Of the 23 sources in Table 1 with identifications, 22 have 2MASS counterparts and their K_s magnitudes are in the range $K_s = 6.3 - 14.1$. The X-ray positions in Table 1 have been registered against 2MASS and the mean positional offset between the X-ray sources and their assigned counterparts is only $0.8''$. A view of the harder X-ray sources in the cluster is seen in the 4 - 7 keV image (Figure 2). The most prominent hard-band detections are a source lying within $1''$ of IRS-1 (source 13 = XMM J054704.78+002143; Figs. 2 and 3), a source associated with 2MASS J054705.25+002253 (source 16), a close X-ray pair lying near the position of IRAS 05445+0016 (sources 20 and 21; Fig. 4), and variable X-rays (Fig. 5) from the emission-line star LkH α 308 (source 19). These hard sources are discussed further below.

Sufficient counts were present in 21 sources to obtain fits of the X-ray spectra with either one-temperature (1T) or two-temperature (2T) *apec* optically thin plasma models. The absorbed fluxes for these objects based on spectral fits are given in Table 1 and fluxes for fainter sources were estimated using PIMMS². Two-temperature models gave acceptable fits of 10 of the brightest sources, excluding source 13 which is discussed in detail below (Sec. 4). These 10 sources (source numbers 1,4,8,12,14,18,19,20,21,29) gave a median hydrogen column density $\log N_H = 22.0 \text{ cm}^{-2}$ and median plasma temperatures $kT_1 = 0.74 \text{ keV}$ and $kT_2 = 2.8 \text{ keV}$. The means are nearly identical to the medians.

3.1. The NGC 2071-IR Region

Figure 3 shows the summed MOS1+2 image of the NGC 2071-IR region known to contain embedded massive young stars. An unusual X-ray source (source 13) is nearly coincident with IRS-1. Its offset from the VLA position of IRS-1 (Torrelles et al. 1998) and the near-IR source 2MASS J054704.78+002142 is only $0.''7$. Thus, an association of this X-ray source with IRS-1 is likely. A search of the HEASARC galaxies data base³ revealed no known galaxies or AGNs within $20''$ of the IRS-1 position so the probability of a chance association between this X-ray source and a distant background object is small. A catalogued VLA 20 cm radio source NVSS J054705.01+002147.2 lies $5.''1$ northeast of the X-ray peak and is most probably associated with IRS-5, which is offset by only $0.''7$ from the VLA source.

The X-ray source located within $1''$ of IRS-1 has 262 net pn counts (0.5 - 7.5 keV; R_e

²Further information on the Portable Interactive Multi-Mission Simulator (PIMMS) can be found at <http://heasarc.gsfc.nasa.gov/docs/software/tools/pimms.html>.

³<http://heasarc.gsfc.nasa.gov/cgi-bin/W3Browse/w3browse.pl>

= 15") and its mean photon energy $\langle E \rangle = 4.62$ keV is the highest of any source in Table 1. Not only is it visible in the 4 - 7 keV hard-band image (Fig. 2), it is also seen in images restricted to the higher 8 - 12 keV range. No large amplitude flare-like variability is seen in the X-ray light curve of this source (Fig. 6) but fluctuations at the $\approx 2\sigma$ level are present. A χ^2 test using the pn light curve gives a probability of constant count rate rate $P_{const} = 0.13$ ($\chi^2/\text{dof} = 19.8/14$; bin size = 2000 s), so no significant variability can be claimed. Fainter X-ray emission is visible in Figure 3 extending to the northeast of IRS-1 that may be associated with IRS-2 ($\delta = 11.''4$), IRS-3 ($\delta = 5.''6$), or IRS-5 ($\delta = 6.''2$) where the offsets δ are relative to IRS-1. In addition, faint emission is present near the position of HH 437 (Zhao et al. 1999) which lies $\approx 15''$ northeast of IRS-1. Higher angular resolution images will be needed to make unambiguous identifications for this fainter emission.

3.2. The IRAS 05445+0016 Region

The luminous far-IR source IRAS 05445+0016 is located $\approx 4'$ south of IRS-1, but with rather large IRAS position uncertainties (Fig. 4). This region is of interest because of reported maser detections in the vicinity (e.g. source Onsala 59 in Harju et al. 1998). The IRAS source was listed as a candidate pre-main sequence object by Clark (1991). Additional far-IR scans of NGC 2071 at 50 μm and 100 μm were obtained with the *Kuiper Airborne Observatory* by Butner et al. (1990).

A close pair of 2MASS sources separated by $\approx 15''$ lies on either side of the IRAS position (Fig. 4) and both were detected by *XMM-Newton* (sources 20 and 21). Both sources are visible in the hard-band image (Fig. 2). The southern source (source 20 = XMM J054707.66+001740) has the highest mean count rate of all sources in Table 1. Its X-ray emission is clearly variable as discerned by a slow decay in the pn light curve during the observation. Its pn spectrum shows a hard component including emission from the Fe K complex (≈ 6.7 keV). We were able to obtain a good spectral fit with an absorbed two-temperature optically thin *apec* plasma model with an absorption column density $\log N_{\text{H}} = 21.8 \text{ cm}^{-2}$, plasma temperature components at $kT_1 = 0.87$ keV and $kT_2 = 3.1$ keV, and $\chi^2/\text{dof} = 94.8/97$. The combination of X-ray variability and a high-temperature component ($T_2 \approx 36$ MK) are characteristic of magnetic activity. The northerly source (source 21 = XMM J054707.93+001755) is offset by only $0.''8$ from the B-type star HDE 290861 (V1380 Ori), a known eclipsing binary system with a component separation of $0.''59$ at position angle (PA) $\approx 217^\circ$ (Prieur et al. 2001). Higher spatial resolution observations will be needed to determine whether the X-rays come from the B star itself or the companion.

3.3. LkH α 308

The second brightest X-ray detection in Table 1 is LkH α 308 (source 19 = XMM J054707.29+001932). This $V = 15.6$ mag emission-line star was identified as a probable T Tauri star by Herbig & Kuhi (1963) and H α emission was confirmed by Wiramihardja et al. (1989). It was discovered to be a relatively bright infrared source by Strom, Strom, & Vrba (1976) and 2MASS data give $K_s = 8.3$ mag. LkH α 308 is an X-ray variable as discerned from its pn light curve which shows a slow rise and fall in count rate by a factor of ~ 2 during the observation (Fig. 5). The pn spectrum reveals a faint Fe K emission line and spectral fits with an absorbed two-temperature optically thin plasma model require a hot component at $kT_2 \approx 3.5 - 5$ keV as commonly seen in magnetically active T Tauri stars.

4. X-ray Spectrum of IRS-1

The X-ray spectrum of the source that we associate with NGC 2071-IRS1 is unusual compared to the optically thin plasma spectra typically seen in young stellar objects. As Figure 7 shows, the spectrum is characterized by a nearly flat broad-band continuum that is heavily absorbed below ≈ 1 keV and a strong broad emission line from neutral or near-neutral iron near 6.4 keV. The fluorescent Fe line dominates the spectrum and its intensity and width are exceptional for a young stellar object.

The spectrum in Figure 7 was extracted using a circular region of radius $R_e = 15''$ and may include contributions from the nearby sources IRS-2, IRS-3, and IRS-5, which lie at offsets of $5.''6 - 11.''4$ from IRS-1. However, we were able to recover a nearly identical spectrum including the strong fluorescent Fe line when using a smaller extraction region of radius $R_e = 4''$. The positions of IRS-2, IRS-3, and IRS-5 lie outside this smaller circle and even though there could be some PSF overlap these results suggest that IRS-1 (or an as yet unresolved source within a few arcseconds of IRS-1) is the dominant X-ray contributor.

We attempted to fit the spectrum using a conventional optically thin plasma model with a single absorption component plus a Gaussian line near 6.4 keV. This model ran away to unphysically high temperatures even when multiple temperature components were allowed. However, we were able to fit the spectrum with either (i) an absorbed power-law continuum with a photon power-law index $\alpha_{ph} = +0.55$ plus a Gaussian line centered at $E_{line} = 6.48$ keV ($\chi^2/\text{dof} = 14.3/14$) or (ii) a two-component optically thin plasma model with a cool moderately absorbed component and a hot heavily-absorbed component plus a Gaussian line centered at $E_{line} = 6.43$ keV ($\chi^2/\text{dof} = 10.7/11$). Fit results are summarized in Table 2.

Both the power-law and thermal fits are formally acceptable but the thermal model

provides a better fit of the shape of the spectrum at lower energies between 1 - 2 keV and is easier to justify on physical grounds. Also, the X-ray absorption $\log N_{\text{H}} = 22.0 \text{ cm}^{-2}$ determined from the power-law model corresponds to a visual extinction $A_{\text{V}} = 4.5 \text{ mag}$ (Gorenstein 1975), which is much less than the range $A_{\text{V}} \approx 28 - 51 \text{ mag}$ expected toward IRS-1 if it is an embedded B0 - B5 star (Wa93). The thermal model yields higher absorptions that are consistent with the range expected for IRS-1. However, we do consider the possibility of power-law models further in Section 5.

High (but physically realistic) X-ray temperatures are required by the two-component thermal model to reproduce the broad-band continuum (Table 2). The absorption inferred for the hot component at $kT_2 = 10.8 \text{ keV}$ is $\log N_{\text{H},2} = 23.2 \text{ cm}^{-2}$. This $N_{\text{H},2}$ implies an equivalent visual extinction $A_{\text{V}} \approx 70 \text{ mag}$ (Gorenstein 1975). Thus, the high-temperature source is heavily obscured. The absorption associated with the cooler component at $kT_1 = 0.7 \text{ keV}$ is $\log N_{\text{H},1} = 22.6 \text{ cm}^{-2}$, or $A_{\text{V}} \approx 17 \text{ mag}$. The strong Fe line accounts for $\approx 30\%$ of the observed (absorbed) flux in the 0.5 - 7.5 keV range. The Gaussian line width deduced from the thermal model $\sigma_{\text{line}} = 140 \text{ eV}$ gives $\text{FWHM} = 330 \text{ eV}$. The line is quite likely resolved since the pn intrinsic energy resolution is $\text{FWHM} \approx 160 \text{ eV}$ at 6.5 keV.

4.1. The Fluorescent Fe Line

The physical picture needed to explain the fluorescent Fe emission requires the presence of neutral or near-neutral material in proximity to the X-ray source. This material is irradiated by the hard source, which is quite likely the embedded high-mass star. The origin of the line broadening is clearly of interest. Velocity broadening of a single line cannot fully account for the line width without invoking unrealistically high velocities. Some of the broadening could be due to multiple closely-spaced Fe lines that are not spectrally distinguishable at the pn energy resolution. In this regard, inspection of the unfolded spectral model shows that a fainter Fe K line may contribute to some of the flux near 6.7 keV but this line, if present, is masked by the broad wings of the 6.43 keV fluorescent line.

If the broad fluorescent line width is a column density effect then the inferred column density is large. The line equivalent width (EW) is related to the column density of cold fluorescent material in the optically thin slab approximation by $\text{EW} \approx 2.3 N_{24} \text{ keV}$ (Kallman 1995), where N_{24} is the column density of the cold matter in units of 10^{24} cm^{-2} . In the present case, our pn spectrum measurements give $\text{EW} = 2.4 \text{ keV}$ so $N_{\text{H,cold}} \sim 10^{24.0} \text{ cm}^{-2}$. The lower signal-to-noise ratio MOS spectra give a somewhat smaller value $\text{EW} = 1.4 \text{ keV}$ or $N_{\text{H,cold}} \sim 10^{23.8} \text{ cm}^{-2}$. The value determined from the pn spectrum is at the upper limit where Kallman's approximation breaks down but if the 6.43 keV feature is a blend then the

inferred value of $N_{\text{H,cold}}$ is only an upper limit.

The above approximation indicates that the absorption column of the cold material is about an order of magnitude greater than the absorption inferred for the hard thermal X-ray component (Table 2). The material responsible for absorption of the hard X-rays cannot fully account for $N_{\text{H,cold}}$ (see also eq. [4] of Tsujimoto et al. 2005). Thus, the cold fluoresced material may not lie directly on the line-of-sight. One possibility is that the fluorescent line originates in the dense ridge of molecular gas orthogonal to the outflow axis which may be a rotating disk (Bally 1982; Seth, Greenhill, & Holder 2002).

Fluorescent Fe line analysis similar to that above has been undertaken on YSOs in other high-mass star-forming regions. Of particular relevance is the *Chandra* study of the Sgr B2 giant molecular cloud by Takagi, Murakami, & Koyama (2002), who reported high-temperature plasma and strong 6.4 keV line emission for some luminous X-ray sources. Specifically, they obtained $kT \approx 10$ keV and a fluorescent Fe line equivalent width $EW = 630$ (180 - 1100; 90% confidence) eV for Sgr B2 source 10 (CXO J174720.2–282305). Takagi et al. note that this X-ray source lies near an ultracompact HII region and may correspond to a massive YSO. The X-ray temperature reported for Sgr B2 source 10 is similar to what we infer for the hot component of NGC 2071 IRS1, but the fluorescent line equivalent width and derived value of $N_{\text{H,cold}}$ is $\approx 3 - 4$ times larger for IRS1.

5. Discussion

The unusual X-ray spectrum of the source near the massive young star IRS-1 warrants further discussion. The presence of cool and hot plasma components apparently seen through different absorption columns suggests that more than one source or X-ray emission process contributes to the spectrum. We consider possible emission processes below.

5.1. Similarities with Jet-Driving T Tauri Stars

The need to invoke two thermal X-ray components at different absorption columns to fit X-ray spectra has also recently been seen in some accreting *low-mass* pre-main sequence stars such as the T Tauri star DG Tau A (Güdel et al. 2005). High-resolution *Chandra* images reveal a two-component X-ray source consisting of a relatively hard strongly-absorbed point source at the stellar position and softer less-absorbed X-ray emission extending along a bipolar jet several arcseconds from the star. The jet is also seen in the optical. Spectral extractions centered on the star capture emission from both components, resulting in a

double-absorption spectrum. Some of the softer emission is due to the shocked jet while the harder point-like emission at the position of DG Tau A is undoubtedly of magnetic origin.

It is conceivable that a similar phenomenon could be responsible for the double-absorption X-ray spectrum detected here for IRS-1. It is unavoidable that our spectral extraction captures a rather large region around the X-ray source and could sample shocked wind or outflow emission that is offset by several arc-seconds from the central source. At $d = 400$ pc, the *XMM-Newton* PSF (FWHM $\approx 4.''3$) corresponds to FWHM ≈ 1700 AU and our nominal source extraction radius $R_e = 15''$ corresponds to a radius of 6000 AU (0.03 pc). The velocity of the bipolar molecular outflow (≈ 70 km s $^{-1}$; Bally 1982) is too low to produce shock-heated plasma at the temperatures inferred from the X-ray spectral fits. However, a higher velocity stellar wind or jet could suffice. The presence of a compact HII region and luminosity considerations suggest that IRS-1 may be an embedded \sim B0 - B5 star (Wa93) which could indeed have already developed a strong wind. Also, IRS-3 lies within our $R_e = 15''$ extraction region and it is known to have a radio jet (Torreles et al. 1998).

Simple shock-heating models (Krolik & Raymond 1985; Raga et al. 2002) give a predicted shock temperature $T_s \approx 1.5 \times 10^5 (v_s/100 \text{ km s}^{-1})^2$ K, where v_s is the shock speed relative to the upstream flow. In order to reach X-ray temperatures comparable to that of the cool X-ray component $T_1 = 8.7$ [2.3 - 11.6] MK (Table 2), shock speeds $v_s \approx 760$ [390 - 880] km s $^{-1}$ would be required. These are fast shocks but perhaps within reason if IRS-1 is an embedded early B-type star. The above shock speed is only about half the terminal wind speed of a B3 V star and about one-third that of a B0 V star (Table 4 of Cassinelli et al. 1994).

5.2. Comments on X-rays from Wind Shocks

X-rays from radiation-driven wind shocks in early-type stars are predicted on theoretical grounds (Lucy 1982; Lucy & White 1980). The expected X-ray temperatures are <1 keV so this process could at best account only for the cooler plasma seen in the two-component spectrum. However, the moderately high X-ray absorption, plasma temperature, and required shock speed for the cool X-ray component noted above stretch the limits of what the radiative wind shock model can accommodate.

A more interesting possibility is that the *hot* plasma is shock related. The impact of a high-velocity wind or jet-like outflow from IRS-1 on a close companion or other obstruction could produce high-temperature X-ray plasma in a colliding wind shock. The colliding wind picture is usually invoked to explain high-temperature X-ray emission in massive close

binaries such as WR + O systems (e.g. Skinner et al. 2001), but in the present case the high-speed wind of the embedded star might actually be shocking on dense surrounding material. Interestingly, Seth et al. (2002) have suggested that the walls of the cavity surrounding IRS-1 might be the interface between outflowing and infalling material. A similar picture in which a high-velocity stellar wind is shocking on dense surrounding clumps has been discussed by Kitamura et al. (1990).

The maximum colliding wind shock temperature in the adiabatic case is $kT_{cw} \approx 1.95 (v_{\perp,s}/1000 \text{ km s}^{-1})^2 \text{ keV}$, where $v_{\perp,s}$ is the velocity component normal to the shock interface (Luo, McCray, & MacLow 1990). Thus, a B0 V star with a terminal wind speed $v_{\infty} \approx 2500 \text{ km s}^{-1}$ could in principle produce very hot X-ray plasma at $kT_{cw} \approx 12 \text{ keV}$, similar to the value $kT_2 \approx 11 \text{ keV}$ inferred for the hot component in the X-ray spectrum (Table 2). The colliding wind model, if relevant, would of course need to account for the X-ray luminosity (Table 2). The X-ray luminosity predicted for a colliding wind system is a sensitive function of mass-loss parameters and orbital separation (Luo et al. 1990). In the absence of such information for IRS1, a meaningful comparison with theory cannot be made and the colliding wind scenario thus remains quite speculative.

5.3. Magnetic Processes in Massive Young Stars?

The hard X-ray continuum detected in IRS-1 extends up to at least 8 keV. Such hard emission represents an extreme case for wind-generated shocks but is not uncommon for X-ray emission from magnetic reconnection processes that are observed in low-mass pre-main sequence stars (T Tauri stars) and even some low-mass protostars (Imanishi, Koyama, & Tsuboi 2001).

Some additional support for magnetic behavior in massive young stellar objects comes from the *Chandra* detection of the high-mass embedded object Mon R2 IRS-2 (Kohno et al. 2002). The X-ray absorption, temperature, and X-ray luminosity reported for Mon R2 IRS-2 are strikingly similar to the values we determine for the hot component of NGC 2071 IRS-1. However, the fluorescent Fe line was not seen in Mon R2 IRS-2. More importantly, the X-ray emission of Mon R2 IRS-2 was found to be variable on timescales of a few 10^4 s , as was that of at least two other embedded high-mass YSOs in Mon R2. The presence of such short-term variability in combination with very hot plasma is a strong argument in favor of magnetic processes.

Because of the close similarities in X-ray spectral properties between NGC 2071 IRS-1 and Mon R2 IRS-2 (apart from the lack of fluorescent Fe in the latter), it is quite possible

that their high-temperature X-ray emission arises from similar processes. If the emission is indeed of magnetic origin, then the key questions are whether the emission is due to as yet undetected late-type companions or the massive YSOs themselves. If the emission is intrinsic to the embedded high-mass objects, then the theoretical challenge will be to determine if the fields are internally generated (and by what mechanism), or instead primordial.

5.4. X-rays from Inverse Compton Scattering

In conclusion, we comment briefly on the possibility that the X-ray continuum emission of the hard source near IRS-1 is nonthermal. As we have noted, the spectrum can be fitted with an absorbed power-law continuum plus a Gaussian Fe line (model B in Table 2), but the inferred absorption is much less than expected toward IRS-1. The production of nonthermal X-rays from OB star winds has been considered by Chen & White (1991). In their model, hard X-rays above 2 keV can be produced by inverse Compton scattering of stellar UV photons by relativistic electrons accelerated in wind shocks near the star.

To explore the nonthermal possibility further, we fitted the pn X-ray spectrum with a model consisting of an absorbed cool thermal component and an absorbed power-law component plus a Gaussian line. The cool thermal component is intended to model any soft radiative wind shock emission and the power-law component models nonthermal emission from inverse Compton scattering. Different absorption columns were allowed for the thermal and power-law components. This model gives a statistically acceptable fit of the spectrum ($\chi^2/\text{dof} = 11.3/11$) with a cool thermal plasma temperature $kT_1 \approx 0.2$ keV and a photon power-law index $\alpha_{ph} = +0.6$. However, the fit converges to a very large emission measure for the cool thermal component which leads to a high unabsorbed luminosity $L_X \sim 10^{34}$ ergs s^{-1} . The inferred presence of a very soft thermal component with extremely high emission measure viewed under high absorption $\log N_{H,1} \approx 22.9$ cm^{-2} is likely a result of fitting the data with an inappropriate model and the fit results seem unphysical. We thus do not favor such a hybrid thermal + nonthermal emission model based on the existing data but the model would be worth reconsidering if higher quality spectra are obtained.

6. Summary and Outlook

We have presented results of the first X-ray observation centered on the core region of the infrared cluster in NGC 2071. The most important (and unanticipated) result of this study is the unusual X-ray spectrum of the source detected within $1''$ of the massive young

stellar object IRS-1. The small positional offset and strong X-ray absorption inferred from thermal spectral models make an association of this X-ray source with IRS-1 likely.

The high X-ray temperature implied by thermal models is characteristic of magnetic processes and raises the intriguing possibility that magnetic fields play an important role in X-ray production in young high-mass stars. Kohno et al. (2002) were led to a similar conclusion based on *Chandra* observations of massive young stars in Mon R2. However, the role played by any as yet unresolved close companions in the X-ray emission process is unknown.

A higher resolution *Chandra* observation of NGC 2071-IR now pending will answer several key questions regarding the origin of the unusual X-ray emission. Specifically, *Chandra*'s arc-second resolution will place tighter constraints on the position of the X-ray peak relative to IRS-1 and will determine if nearby objects such as IRS-2, IRS-3, or IRS-5 contribute to the X-ray emission. The longer *Chandra* exposure will also provide a more definitive test for variability on short timescales, a key discriminant between magnetic and shock processes.

REFERENCES

- Anders, E. & Grevesse, N. 1989, *Geochim. Cosmochim. Acta*, 53, 197
- Anthony-Twarog, B. 1982, *AJ*, 87, 1213
- Aspin, C., Sandell, G., & Walther, D.M. 1992. *MNRAS*, 258, 684
- Bally, J. 1982, *ApJ*, 261, 558
- Brown, A.G.A., de Geus, E.J., & de Zeeuw, P.T. 1994, *A&A*, 289, 101
- Butner, H.M., Evans, N.J., Harvey, P.M., Mundy, L.G., Natta, A., & Randich, M.S. 1990, *ApJ*, 364, 164
- Cassinelli, J.P., Cohen, D.H., MacFarlane, J.J., Sanders, W.T., & Welsh, B.Y. 1994, *ApJ*, 421, 705
- Chen, W. & White, R.L. 1991, *ApJ*, 366, 512
- Clark, F.O., 1991 *ApJS*, 75, 611
- Gorenstein, P., 1975 *ApJ*, 198, 95
- Güdel, M., Skinner, S.L., Briggs, K.R., Audard, M., Arzner, K., & Telleschi, A. 2005, *ApJ*, 626, L53

- Harju, J. et al., 1998 A&AS, 132, 211
- Herbig, G.H. & Kuhi, L.V. 1963, ApJ, 137, 398
- Imanishi, K., Koyama, K., & Tsuboi, Y. 2001, ApJ, 557, 747
- Kallman, T.R., 1995, ApJ, 455, 603
- Kitamura, Y., Kawabe, R., Yamashita, T., & Hayashi, M., 1990 ApJ, 363, 180
- Kohno, M., Koyama, K., & Hamaguchi, K. 2002, ApJ, 567, 423
- Krolik, J.H. & Raymond, J.C. 1985, ApJ, 298, 660
- Lada, E.A., DePoy, D.L., Evans, N.J., & Gatley, I., 1991 ApJ, 371, 171
- Lucy, L.B. 1982, ApJ, 255, 286
- Lucy, L.B. & White, R.L. 1980, ApJ, 241, 300
- Luo, D., McCray, R., & MacLow, M.-M. 1990, ApJ, 362, 267
- Prieur, J.-L., Oblak, E., Lampens, P., Kurpinska-Winiarska, M., Aristidi, E., Koechlin, L., & Ruymaekers, G. 2001, A&A, 367, 865
- Raga, A.C., Noriega-Crespo, A., & Velázquez, P.F. 2002, ApJ, 576, L149
- Seth, A.C., Greenhill, L.J., & Holder, B.P. 2002, ApJ, 581, 325
- Skinner, S.L., Güdel, M., Schmutz, W., & Stevens, I.R. 2001, ApJ, 558, L113
- Snell, R.L. & Bally, J. 1986, ApJ, 303, 683
- Strom, K.M., Strom, S.E., & Vrba, F.J. 1976, AJ, 81, 308
- Strüder, L. et al. 2001, A&A, 365, L18
- Takagi, S.-I., Murakami, H., & Koyama, K., 2002, ApJ, 573, 275
- Torrelles, J.M., Gómez, J.F., Rodríguez, L.F., Curiel, S., Anglada, G., & Ho, P.T.P. 1998, ApJ, 505, 756
- Tsujimoto, M. et al. 2005, ApJS, 160, 503
- Turner, M.J.L. et al. 2001, A&A, 365, L27
- Walther, D.M., Robson, E.I., Aspin, C., & Dent, W.R.F. 1993, ApJ, 418, 310 (Wa93)

Wiramihardja, S.D., Kogure, T., Yoshida, S., Ogura, K., & Nakano, M. 1989, PASJ, 41, 155

Zhao, B. et al. 1999, AJ, 118, 1347

This research was supported by NASA grants NNG05GK52G and NNG05GE69G. Work at PSI (M.G.) was supported by Swiss National Science Foundation grant 20-66875.01. M.A. acknowledges support from NASA grant NNG05GK35G and a Swiss National Science Foundation Professorship (PP002-110504). This work is based on observations obtained with *XMM-Newton*, an ESA science mission with instruments and contributions directly funded by ESA states and the USA (NASA). We have utilized data products from the Two Micron All-Sky Survey (2MASS), which is a joint project of the University of Massachusetts and IPAC/CalTech.

Table 1. X-ray Sources in NGC 2071^a

No.	R.A. (J2000)	Decl. (J2000)	Rate (c/s)	<E> (keV)	Flux (ergs/cm ² /s)	Identification	K _s (mag)	offset (")
1	05 46 44.10	+00 18 02.6	1.49E-02	1.66	8.18E-14	2MA J054644.08+001803	10.2	0.6
2	05 46 44.91	+00 24 51.3	5.69E-04	2.33	1.03E-14 ^e
3	05 46 45.84	+00 17 00.3	1.87E-03	2.34	1.46E-14
4	05 46 51.51	+00 19 20.9	1.34E-02	1.68	6.18E-14	2MA J054651.48+001921	11.8	0.6
5 ^d	05 46 51.80	+00 19 39.4	1.46E-03	1.89	1.99E-14 ^e	2MA J054651.85+001938	11.6	1.1
6 ^c	05 46 52.51	+00 19 59.2	6.02E-04	1.80	1.64E-14 ^e
7	05 46 53.47	+00 26 32.3	8.70E-04	2.62	4.81E-15 ^e
8	05 46 56.56	+00 20 52.5	1.07E-02	1.97	4.81E-14	2MA J054656.53+002052	10.6	0.5
9 ^b	05 46 58.46	+00 22 35.3	4.98E-04	1.93	6.80E-15 ^e	2MA J054658.37+002236	14.1	1.7
10	05 46 58.71	+00 20 29.0	3.04E-03	2.04	1.02E-14	Wa93-51; 2MA J054658.59+002029	12.2	1.8
11	05 46 59.03	+00 24 57.8	1.44E-03	3.27	1.74E-14	2MA J054659.03+002457	12.4	0.1
12	05 47 03.38	+00 23 23.5	1.98E-02	2.29	1.39E-13	2MA J054703.31+002323	10.4	1.0
13	05 47 04.78	+00 21 43.5	8.77E-03	4.62	1.29E-13	IRS-1; 2MA J054704.78+002142	11.2	0.7
14	05 47 05.00	+00 18 32.0	1.76E-02	1.88	8.92E-14	2MA J054704.94+001831	10.4	0.9
15 ^b	05 47 05.21	+00 23 08.4	4.02E-03	2.64	7.01E-14
16 ^h	05 47 05.27	+00 22 53.7	2.41E-02	3.19	1.94E-13	2MA J054705.25+002253	12.4	0.3
17 ^b	05 47 05.56	+00 22 11.4	9.30E-04	2.87	1.27E-14 ^e
18	05 47 06.26	+00 24 53.5	2.30E-02	2.51	1.74E-13	2MA J054706.26+002454	10.7	0.5
19	05 47 07.29	+00 19 32.0	5.79E-02	2.70	4.27E-13	Lk308, 2MA J054707.26+001932	8.3	0.4
20	05 47 07.66	+00 17 40.9	1.11E-01	2.01	5.79E-13	2MA J054707.64+001740	8.8	0.3
21 ^d	05 47 07.93	+00 17 55.5	1.30E-02	1.74	1.60E-13	2MA J054707.91+001756 ^f	6.3	0.5
22	05 47 08.92	+00 20 26.5	2.17E-03	2.50	1.20E-14 ^e
23	05 47 09.77	+00 22 35.5	5.55E-03	2.90	4.71E-14	2MA J054709.77+002236	12.0	0.5
24	05 47 10.21	+00 20 08.9	1.74E-03	3.11	9.62E-15 ^e	... ^g
25 ^c	05 47 10.33	+00 17 22.2	1.73E-03	2.29	2.36E-14 ^e	2MA J054710.36+001721	12.0	0.7
26	05 47 10.59	+00 18 44.3	2.11E-03	2.16	8.37E-15	USNO J054710.63+001845	...	1.3
27	05 47 10.70	+00 26 19.9	5.02E-04	3.24	2.78E-15 ^e
28	05 47 10.91	+00 19 14.9	3.31E-03	2.13	1.82E-14	Lk310, 2MA J054710.98+001914	9.1	1.1
29	05 47 12.03	+00 17 57.6	8.87E-03	1.97	6.93E-14	2MA J054712.02+001756	10.6	0.8
30 ^c	05 47 12.95	+00 22 06.4	2.59E-03	2.40	3.41E-14	2MA J054712.92+002206	10.5	0.5
31 ^b	05 47 15.51	+00 18 43.2	6.64E-04	3.40	9.06E-15 ^e
32 ^c	05 47 15.86	+00 23 21.4	9.63E-04	3.26	1.31E-14 ^e	2MA J054715.92+002320	13.3	1.4
33	05 47 19.27	+00 19 19.5	1.91E-03	2.26	6.04E-15	2MA J054719.19+001920	11.7	1.7

^aNotes: Data are from the *XMM-Newton* observation on 30-31 March 2005 and include sources within a $\approx 10' \times 10'$ region centered on NGC 2071-IRS1. All quantities are computed using events in the 0.5 - 7.5 keV range. Usable exposure times are 29,886 s for pn and 30,114 s per MOS. Data are from EPIC pn unless otherwise noted. The count rate is based on events extracted within a circular region of radius 15" (68% EEF) centered on the source and is background subtracted. A smaller source region of radius $\approx 10''$ was used for sources 5,16, and 21 due to source crowding. The absorbed flux (0.5 - 7.5 keV) is based on spectral fits using an absorbed solar-abundance 1T or 2T optically thin plasma model (*apec*) in XSPEC, except as noted for faint sources. <E> is the mean photon energy. Candidate identifications lie within 2" of the X-ray position and are based (in order of preference) on searches of the 2MASS (2MA), HST GSC v2.2, and USNO B1 electronic data bases. The 2MASS K_s magnitude is given for sources with 2MASS identifications. The quoted *offset* is the positional offset between the X-ray and 2MASS or USNO positions.

^bBased on MOS2 events. Source not detected in pn.

^cBased on MOS2 events. Source lies near pn CCD gap.

^dBased on MOS2 events. Second source lies nearby.

^eAbsorbed flux (0.5 - 7.5 keV) is from PIMMS based on the quoted count rate and an assumed Raymond-Smith model with $N_{\text{H}} = 10^{22} \text{ cm}^{-2}$ and plasma temperature $kT = 2 \text{ keV}$.

^fThe star HDE 290861 is offset $0.''8$ from the X-ray position.

^gIR source 29 in Walther et al. 1993 is offset by $2.''4$ from the X-ray position.

^hMOS images show a faint source located $\approx 17''$ north of source 16.

Table 2. *XMM-Newton* Spectral Fits for IRS-1

Parameter	A	B
Model ^a	A	B
Emission	thermal + line	power-law + line
N _{H,1} (10 ²² cm ⁻²)	3.8 [2.2 - 10.]	1.0 [0.19 - 2.3]
kT ₁ (keV)	0.75 [0.20 - 1.0]	...
norm ₁ (10 ⁻⁴) ^b	2.1 [0.4 - ...]	0.04 [0.02 - 0.06]
N _{H,2} (10 ²³ cm ⁻²)	1.6 [0.48 - 3.0]	...
kT ₂ (keV)	10.8 [5.8 - ...]	...
norm ₂ (10 ⁻⁴) ^b	1.4 [0.76 - 2.3]	...
α _{ph}	...	0.55 [0.26 - 0.85]
E _{line} (keV)	6.43 [6.37 - 6.53]	6.48 [6.42 - 6.54]
σ _{line} (keV)	0.14 [0.06 - 0.26]	0.21 [0.14 - 0.28]
norm _{line} (10 ⁻⁶)	4.5 [2.9 - 6.5]	5.5 [4.2 - 6.9]
χ ² /dof	10.7/11	14.3/14
χ _{red} ²	0.97	1.02
F _X (10 ⁻¹³ ergs cm ⁻² s ⁻¹)	1.28 (7.93)	1.27 (1.39)
F _{X,1} (10 ⁻¹³ ergs cm ⁻² s ⁻¹)	0.13 (4.99)	...
F _{X,line} (10 ⁻¹⁴ ergs cm ⁻² s ⁻¹)	3.86 (4.03)	3.56 (3.56)
L _X (10 ³¹ ergs s ⁻¹)	1.5	0.27
L _{X,1} (10 ³¹ ergs s ⁻¹)	0.95	...

Note. — Based on XSPEC (vers. 12.3.0) fits of the background-subtracted EPIC pn spectrum binned to a minimum of 15 counts per bin using 29.9 ksec of low-background exposure. Thermal emission was modeled with a solar abundance (Anders & Grevesse 1989) *apec* optically thin plasma model in XSPEC. The tabulated parameters are absorption column density (N_H), plasma energy (kT), component normalization (norm), photon power-law index (α_{ph}), Gaussian line centroid energy (E_{line}), and line width (σ_{line} = FWHM/2.35). Solar abundances are referenced to Anders & Grevesse (1989). Square brackets enclose 90% confidence intervals and an ellipsis means that the algorithm used to compute confidence intervals did not converge. The total X-ray flux (F_X) and flux of the low-absorption component (F_{X,1}) are the absorbed values in the 0.5 - 7.5 keV range, followed in parentheses by unabsorbed values. The continuum-subtracted fluorescent Fe line flux (F_{X,line}) is measured in the 6.2 - 6.6 keV range. The unabsorbed total luminosity L_X (0.5 - 7.5 keV) and cool-component luminosity L_{X,1} (0.5 - 7.5 keV) assume a distance of 400 pc.

^aModel A: N_{H,1}·kT₁ + N_{H,2}·kT₂ + GAUSS; Model B: N_{H,1}·PL + GAUSS

^bFor thermal *vapec* models, the norm is related to the emission measure (EM) by EM = 4π10¹⁴d_{cm}²×norm, where d_{cm} is the stellar distance in cm.

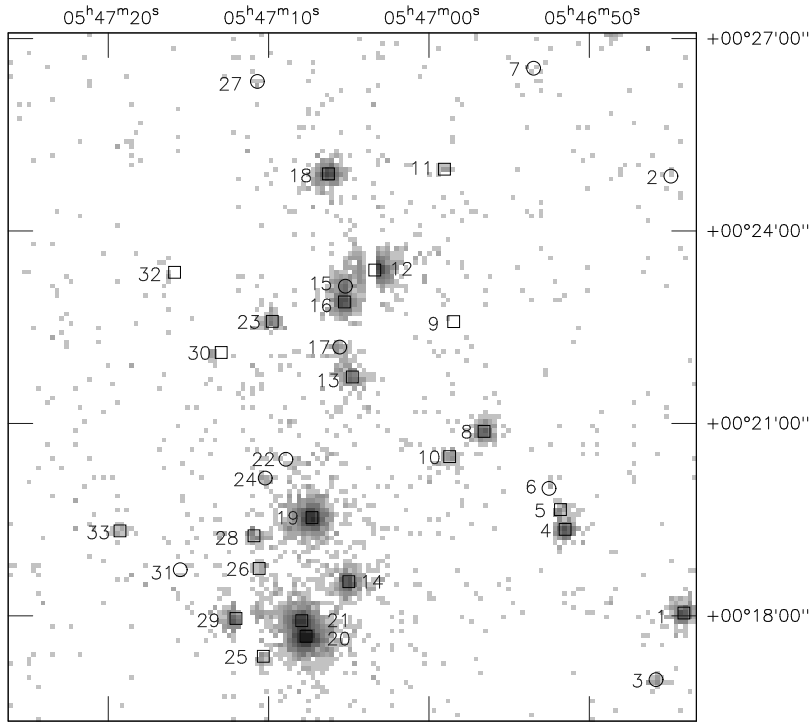


Fig. 1.— Broad-band *XMM-Newton* EPIC pn X-ray image of the $\approx 10' \times 10'$ central region in NGC 2071 (0.5 - 7 keV; 29.9 ksec usable exposure; rebinned to a pixel size of $4.''4$; log scale; J2000.0 coordinates). Numbered X-ray sources correspond to Table 1. Boxes enclose X-ray sources with identified counterparts and circled sources lack counterparts.

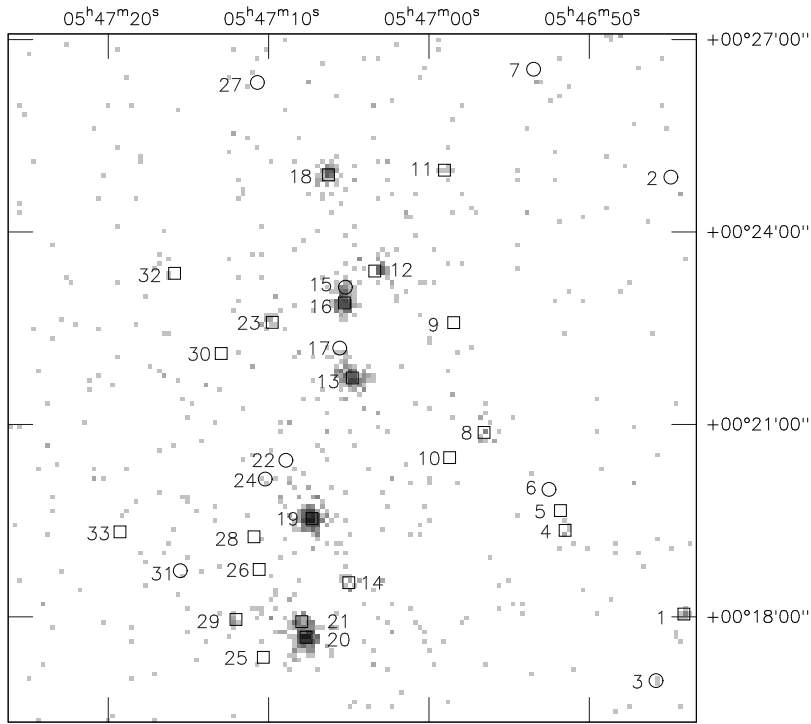


Fig. 2.— Same as Figure 1, but restricted to the hard 4 - 7 keV band.

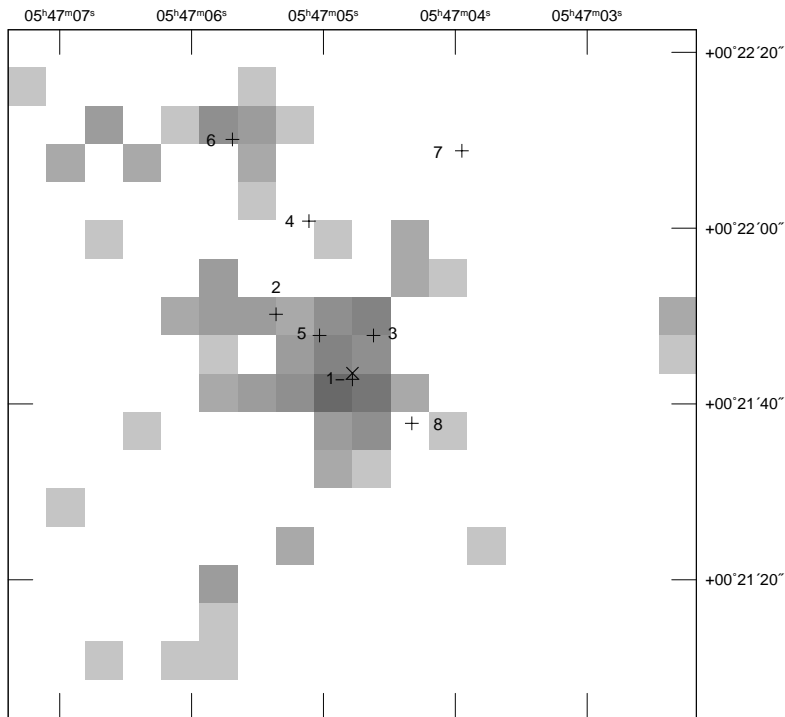


Fig. 3.— Zoomed EPIC MOS1+2 X-ray image of the central NGC 2071-IR subgroup (0.5 - 7 keV; rebinned to a pixel size of $4.''4$; log scale; J2000.0). Crosses show IR positions of IRS 1-8 (Wa93) and \times is the centroid of the X-ray source associated with IRS-1.

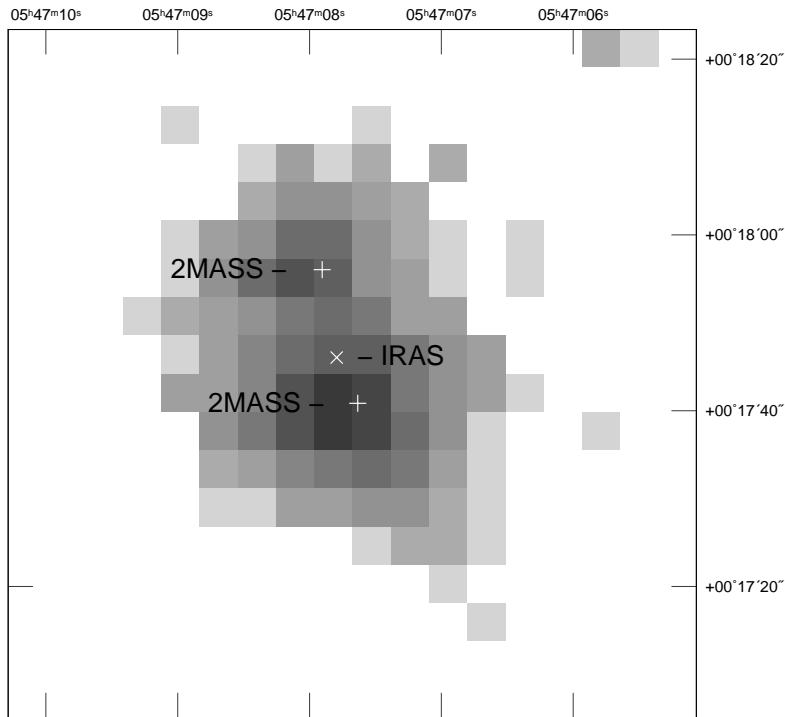


Fig. 4.— EPIC MOS1+2 image (0.5 - 7 keV) of the close pair sources 20 (south) and 21 (north). Positions of 2MASS sources are marked with crosses (+). Source 21 is possibly associated with the B star HDE 290861 (or its close companion) which lies at an offset of $0.''8$ from the X-ray peak. The position of IRAS 05445+0016 (\times) has a 95% uncertainty ellipse of $47'' \times 7''$ (semi-major \times semi-minor axes) with the ellipse major axis at PA = 89° .

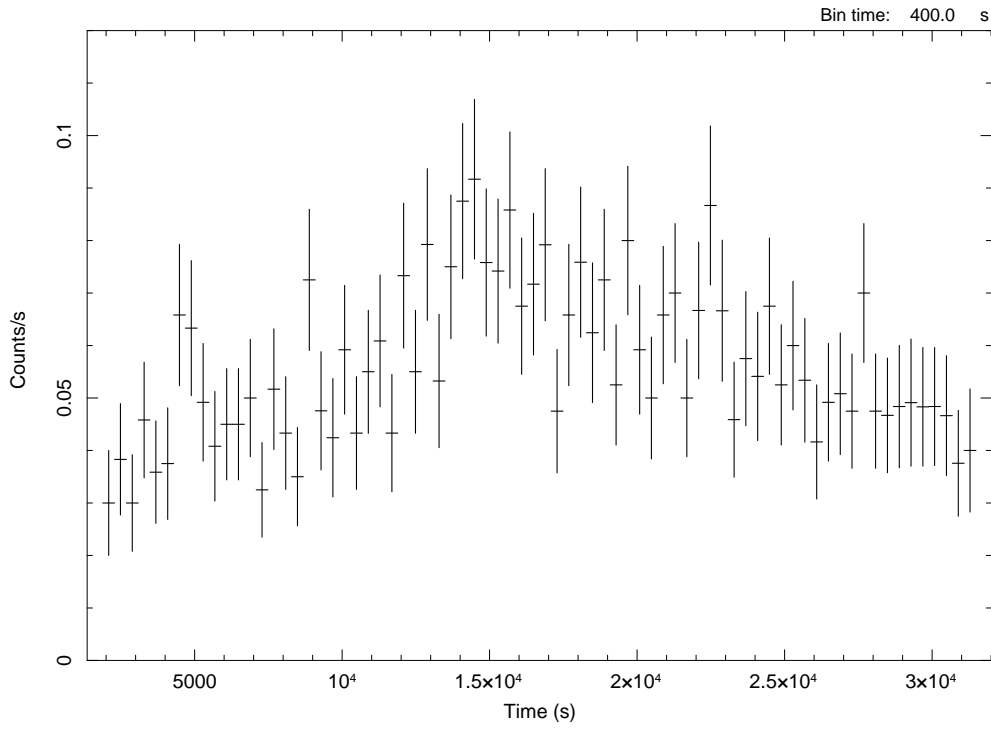


Fig. 5.— Background-subtracted EPIC pn light curve of the emission-line star LkHa 308 (source 19 = XMM J054707.29+001932) in the 0.5 - 7 keV range. The bin size is 400 s.

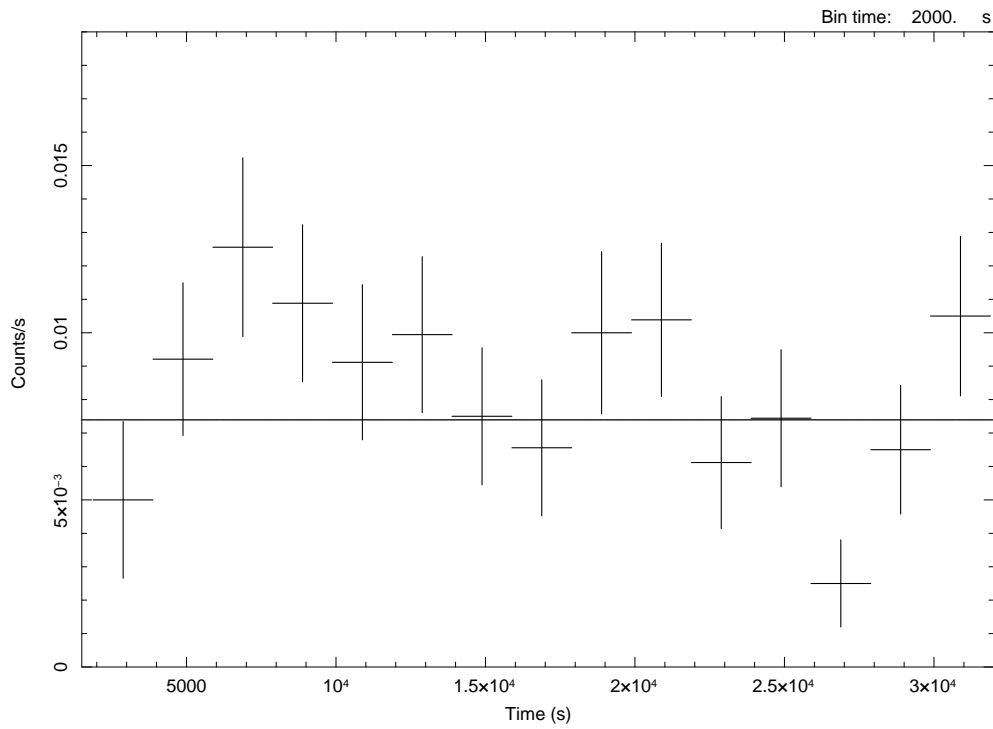


Fig. 6.— Background-subtracted EPIC pn light curve of XMM J054704.78+002143 (offset by $0.''7$ from IRS-1) in the 0.5 - 7 keV range. The bin size is 2000 s and the solid line is a best-fit constant count rate model.

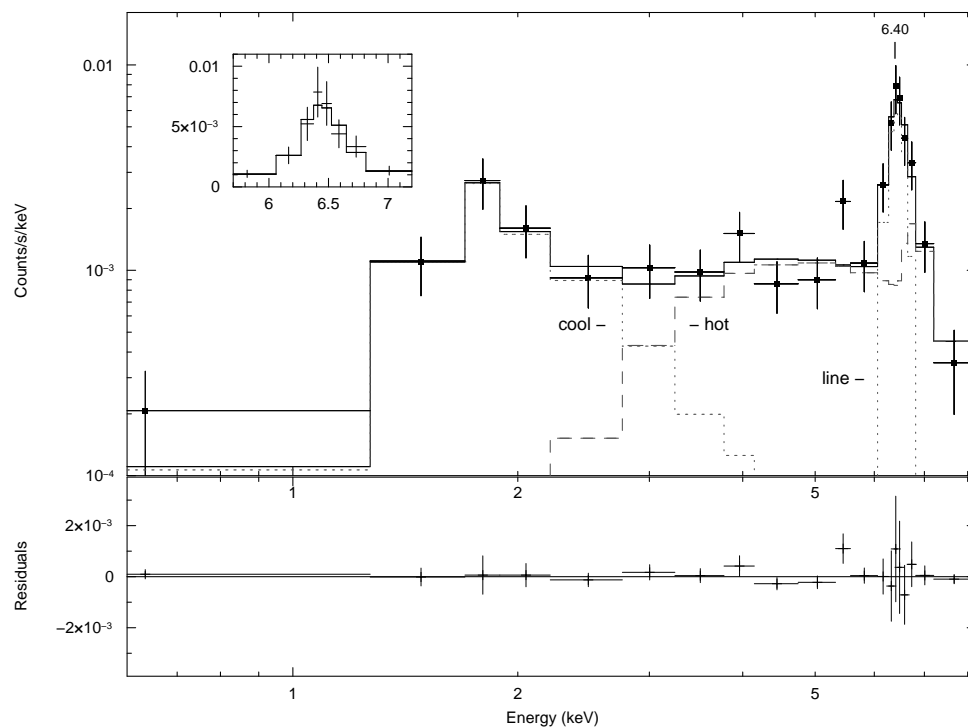


Fig. 7.— Background-subtracted EPIC pn spectrum of XMM J054704.78+002143 (offset by 0.''7 from IRS-1) binned to a minimum of 15 counts per bin (262 net counts in the 0.5 - 7.5 keV range; extraction radius $R_e = 15''$). The spectrum is dominated by a strong fluorescent Fe emission line near 6.4 keV. The solid line is a best-fit double-absorber thermal model (model A in Table 2) with a cool moderately absorbed component (dotted line) and a hot heavily absorbed component (dashed line), plus a Gaussian line (dotted). The inset shows the Fe line on a linear axis scale.